

## Flame-synthesized LaCoO<sub>3</sub>-supported Pd 2. Catalytic behavior in the reduction of NO by H<sub>2</sub> under lean conditions

Gian Luca Chiarello<sup>a</sup>, Davide Ferri<sup>b</sup>, Jan-Dierk Grunwaldt<sup>b</sup>, Lucio Forni<sup>a,\*</sup>, Alfons Baiker<sup>b</sup>

<sup>a</sup> Dipartimento di Chimica Fisica ed Elettrochimica, Università degli Studi di Milano, via C. Golgi 19, I-20133 Milano, Italy

<sup>b</sup> Institute for Chemical and Bioengineering, Department of Chemistry and Applied Biosciences, ETH Zurich, Hönggerberg, HCI, 8093 Zurich, Switzerland

Received 18 July 2007; revised 25 September 2007; accepted 2 October 2007

### Abstract

A 0.5 wt% Pd/LaCoO<sub>3</sub>, prepared by flame-spray pyrolysis (FP), was tested as catalyst for the low-temperature selective reduction of NO by H<sub>2</sub> in the presence of excess O<sub>2</sub>. In particular, the effect of the precalcination and prereduction temperature on catalytic activity was compared with that of a similar Pd/LaCoO<sub>3</sub> sample prepared by impregnation with a Pd solution of FP-prepared LaCoO<sub>3</sub>. The FP-made catalyst allowed full NO conversion at 150 °C, with 78% selectivity to N<sub>2</sub>, thus outperforming the catalytic behavior of the corresponding sample prepared by impregnation. The higher activity of the FP-made catalyst has been attributed to the formation of segregated Co metal particles, not present in the impregnated sample, formed during the precalcination at 800 °C, followed by reduction at 300 °C. Two reaction mechanisms can be deduced from the temperature-programmed experiments. The first of these, occurring at lower temperatures, indicates cooperation between the Pd and Co metal particles, with formation of active nitrates on cobalt, successively reduced by hydrogen spillover from Pd. The second, occurring at higher temperature, allows 50% conversion of NO, with >90% selectivity to N<sub>2</sub>, and involves N adatoms formed by dissociative NO adsorption over Pd. Prereduction at 600 °C led to a slight increase in catalytic activity, due to the formation of a Pd–Co alloy, which is more stable on reoxidation compared with Pd alone. Moreover, the cooperative reaction mechanism seems to be favored by the proximity of Co and Pd in metal particles.

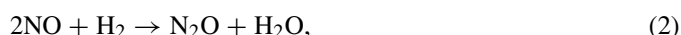
© 2007 Elsevier Inc. All rights reserved.

**Keywords:** Flame-spray pyrolysis; Lean conditions de-NO<sub>x</sub>; Pd/LaCoO<sub>3</sub> perovskite; *In situ* fluorescence EXAFS

### 1. Introduction

Hydrogen is an effective and clean alternative energy carrier. However, the high temperature of hydrogen combustion can lead to an even more abundant formation of NO<sub>x</sub> than in normal fossil fuel combustion. Thus, the catalytic system needed to remove NO<sub>x</sub> from the exhausts of lean-burn systems, using H<sub>2</sub> as a fuel, should be able to selectively reduce NO<sub>x</sub> in the presence of excess oxygen, exploiting the traces of unburnt H<sub>2</sub> present in the same exhaust. Moreover, H<sub>2</sub> represents a valid clean reducer alternative to NH<sub>3</sub>, which is widely accepted as the reducing agent of choice for the selective catalytic reduction (SCR) of NO<sub>x</sub> [1].

We considered the following reactions:



and



Reaction (1) is the desired one; the others are undesired side reactions. In particular, reaction (4) competes with reaction (1), decreasing NO conversion. The competition of reaction (1) with reactions (2) and (3) decreases the selectivity to N<sub>2</sub>.

Over the last two decades, several catalyst formulations have been proposed for selective NO<sub>x</sub> reduction by hydrogen (H<sub>2</sub>-SCR) [2–10]. Among these, perovskite-like mixed oxides appear promising, due to their great versatility and redox properties. Doped perovskites [11,12] were found to be very active

\* Corresponding author. Fax: +39 02 50314300.  
E-mail address: [lucio.forni@unimi.it](mailto:lucio.forni@unimi.it) (L. Forni).

for the H<sub>2</sub>-SCR in the absence of O<sub>2</sub>. A new stimulus was given by Costa et al. [13,14], who reported that Pt supported by impregnation on a perovskite displayed higher NO conversion and selectivity to N<sub>2</sub> at low temperature in the NO/H<sub>2</sub>/O<sub>2</sub> system compared with Pt/ $\gamma$ -Al<sub>2</sub>O<sub>3</sub>. Similarly, it has been reported that the addition of water promoted reduction of NO over Pd/LaCoO<sub>3</sub> without affecting selectivity, whereas an inhibiting effect was observed over Pd/Al<sub>2</sub>O<sub>3</sub> [15]. In addition, Pd-doped perovskites (e.g., LaFe<sub>0.95</sub>Pd<sub>0.05</sub>O<sub>3</sub>) seem to have a sort of self-regenerative character, in which Pd can move into (as Pd<sup>n+</sup>) or out of (as Pd<sup>0</sup>) the framework, depending on the redox fluctuations of exhaust gases, thus preventing sintering of Pd particles [16–18].

Different mechanisms of reaction over noble metal-based catalysts have been proposed. Although all authors agree on the dissociative adsorption of H<sub>2</sub> on noble metals, different interpretations regarding the interaction of NO and its successive reaction with H adatoms to give N<sub>2</sub> (and N<sub>2</sub>O) and H<sub>2</sub>O have been advanced. Burch et al. [19] proposed two routes of N<sub>2</sub> formation over Pt/SiO<sub>2</sub>, passing through chemisorbed N-containing species on the surface of Pd. The latter can react either with gaseous or physisorbed NO through an “impact” route or with another identical N-containing species, each delivering one nitrogen atom to the final product. This mechanism has been confirmed and implemented by Costa and Efstathiou [20], who also compared it with the paths on Pt/La<sub>0.5</sub>Ce<sub>0.5</sub>MnO<sub>3</sub>, thereby demonstrating the important role played by the support chemical composition. It was found that at  $T_{\max} = 140^\circ\text{C}$ , on Pt/SiO<sub>2</sub> the active N species (particularly nitrosyls and unidentate nitrates) was present exclusively on the noble metal particle surface, whereas on Pt/La<sub>0.5</sub>Ce<sub>0.5</sub>MnO<sub>3</sub>, the two active intermediate NO<sub>x</sub> species were nitrosyls and bidentate nitrates, both present on the support surface. The reduction of these intermediate species to N<sub>2</sub> and N<sub>2</sub>O was due to hydrogen spillover from metallic Pt on the support surface. The latter aspect was also reported by Machida et al. over Pd/MnO<sub>x</sub>-CeO<sub>2</sub> [6]. Ueda et al. [4] observed two NO reduction conversion maxima at 100 °C and 300 °C over Pd/TiO<sub>2</sub>, and suggested that at low temperature, NO reacts directly with H<sub>2</sub> over Pd, whereas at high temperature, NO oxidizes to NO<sub>2</sub>, which is subsequently reduced by H<sub>2</sub>. Finally, Qi et al. [9] observed the formation of an intermediate NH<sub>4</sub><sup>+</sup> in the NO/H<sub>2</sub>/O<sub>2</sub> reaction over Pd-V<sub>2</sub>O<sub>5</sub>/TiO<sub>2</sub>-Al<sub>2</sub>O<sub>3</sub>, with NH<sub>4</sub><sup>+</sup> considered responsible for the higher activity of this catalyst with respect to a V<sub>2</sub>O<sub>5</sub>-free sample in which, in contrast, almost no NH<sub>4</sub><sup>+</sup> formation occurs. A plausible intermediate NO–NO dimeric species also has been suggested [20–23], forming either onto the metal cation sites or on oxygen vacancies.

Flame pyrolysis (FP) is a low-cost, continuous single-step method recently optimized by our group for perovskite preparation [24,25]. Whereas the FP preparation of noble metal on single oxides has been demonstrated [26–28], some difficulties have arisen in the direct synthesis of noble metals supported on perovskite, due to the possible replacement of the noble metal for the cation at the B site of the ABO<sub>3</sub> perovskite framework [16,29,30]. Indeed, FP is an effective technique for the synthesis of doped perovskite-like mixed oxides [29,31]. This

problem can be overcome by properly setting the FP operation parameters, that is, by adjusting the organic solvent composition governing the flame temperature, taking into account the possible noble metal cation mobility, leading to the surface segregation of noble metal particles.

In an accompanying contribution [32], we reported the structural changes occurring in the FP-made catalyst on calcination and reduction, namely particle sintering, Pd and Co segregation, formation of a Pd–Co alloy, and irreversible reduction of the support to La<sub>2</sub>O<sub>3</sub> + Co. The aim of the present work was to investigate the effect of these changes on the catalytic activity for H<sub>2</sub>-SCR under lean-burn conditions in the temperature range 50–450 °C, by comparing a FP-prepared 0.5 wt% Pd/LaCoO<sub>3</sub> (PdLCO) with a 0.5 wt% Pd/LaCoO<sub>3</sub> (impPdLCO) prepared by the traditional Pd impregnation of a FP-made LaCoO<sub>3</sub>. In situ X-ray absorption near-edge structure (XANES) and extended X-ray absorption fine structure (EXAFS) around the Pd K-edge were performed to investigate the structural changes intervening in the catalyst during reaction between 50 and 500 °C. Finally, transient experiments, namely NO temperature-programmed desorption (NO-TPD) in flowing He and temperature-programmed surface reaction (TPRS) in flowing H<sub>2</sub>/He or H<sub>2</sub>/O<sub>2</sub>/He, were performed to collect information about the possible reaction mechanism.

## 2. Experimental

### 2.1. Catalyst preparation

The PdLCO catalyst was prepared by FP, as described in detail in our accompanying study [32]. In brief, La(CH<sub>3</sub>COO)<sub>3</sub>·*x*H<sub>2</sub>O (Aldrich, purity > 99.9%, 7.5 wt% H<sub>2</sub>O, determined by TGA), Co(CH<sub>3</sub>COO)<sub>2</sub>·4H<sub>2</sub>O (Merck, purum), and Pd(CH<sub>3</sub>COO)<sub>2</sub> (Fluka, purum) in the desired ratios and 0.15 M overall concentration, referred to La or Co ions, were dissolved in a mixture of propionic acid, *n*-propanol, and water (5:4:1 vol%). The solution thus obtained was fed at a rate of 4 mL/min to the nozzle of a vertical burner, along with 5 L/min of O<sub>2</sub>. The spray was ignited and sustained by a premixed methane/oxygen flame issuing from an annular ring surrounding the nozzle. The pressure drop of oxygen across the nozzle was kept constant at 1 bar, to ensure a sonic flow regime [24]. The produced particles were collected on a glass fiber filter connected to a vacuum pump. Two catalysts were prepared for comparison: a FP-made LaCoO<sub>3</sub> (LCO), synthesized using the same parameters of PdLCO and a 0.5 wt% Pd/LaCoO<sub>3</sub> (impPdLCO), prepared by the traditional impregnation method, by depositing Pd from a (NH<sub>4</sub>)<sub>2</sub>PdCl<sub>4</sub> (Fluka, puriss) solution on LCO, preannealed at 800 °C. The impregnated catalyst was then first dried overnight at 90 °C and then calcined at 500 °C for 2 h in flowing 10% O<sub>2</sub>/He (30 mL/min) gas mixture.

### 2.2. Catalytic activity

Catalytic activity tests for the selective reduction of NO by H<sub>2</sub> in the presence of excess O<sub>2</sub> were carried out by a bench-scale continuous reaction unit, including a U-shaped tubular

quartz reactor (i.d. = 7 mm) heated by an electric furnace (Carbolite, model MTF 12/38A). The reactor temperature was measured by a thermocouple placed in a thin quartz tube beside the catalyst bed. The catalyst (ca. 0.15 g, 0.20–0.30 mm particle size, diluted 1:4 by weight with quartz powder of the same particle size) was loaded between two flocks of quartz wool. Before each run, the catalyst was activated at 600 or 800 °C for 2 h in flowing 10% O<sub>2</sub>/He (20 cm<sup>3</sup>/min), then cooled to 40 °C in the same gas flowing mixture. If not stated otherwise, a reduction in flowing 10% H<sub>2</sub>/He (20 mL/min) followed, while temperature was increased to either 300 or 600 °C at 10 °C/min. The activity tests were carried out by feeding a mixture composed of 0.25 vol% NO, 1 vol% H<sub>2</sub>, 5 vol% O<sub>2</sub> (He balance) at 100 mL/min overall flow rate, while increasing temperature up to 450 °C by 2 °C/min.

The reactor outlet was connected to an HP micro GC (model M200H), equipped with PoraPLOT U and MS-5A PLOT columns. The former was used for H<sub>2</sub>, O<sub>2</sub>, N<sub>2</sub>, and NO quantification; the latter, for N<sub>2</sub>O. The composition of the gas phase was monitored with an Omnistar Pfeiffer Vacuum GSD 30102 quadrupole mass spectrometer (QMS) connected to the reactor outlet through a stainless steel capillary tube kept at ca. 150 °C. The NO mol% conversion ( $X_{\text{NO},T}$ ), defined as the ratio of reacted over fed NO, and the percent selectivity to N<sub>2</sub> ( $S_{\text{N}_2,T}$ ), defined as the ratio of twice the moles of produced N<sub>2</sub> over the moles of reacted NO, at temperature  $T$ , were calculated by the following equations:

$$X_{\text{NO},T} = \frac{A_{\text{NO},0} - A_{\text{NO},T}}{A_{\text{NO},0}} \times 100$$

and

$$S_{\text{N}_2,T} = \frac{2\alpha A_{\text{N}_2,T}}{C_{\text{NO},0} X_{\text{NO},T}} \times 100,$$

where  $A_{\text{NO},0}$  is the NO chromatographic peak area, measured on the feeding gas when bypassing the reactor;  $A_{\text{NO},T}$  and  $A_{\text{N}_2,T}$  are the NO and N<sub>2</sub> chromatographic peak areas, respectively, measured on the outlet gas at reaction temperature  $T$ .  $C_{\text{NO},0}$  is the NO concentration (= 0.25 vol% in this case) in the feeding gas, and  $\alpha$  is the slope of the titration curve of the chromatographic peaks of N<sub>2</sub>. Thus,  $\alpha A_{\text{N}_2,T}$  represents the vol% concentration of N<sub>2</sub> produced at temperature  $T$ .

The effect of pretreatment conditions on catalytic activity was investigated on samples labeled (Pd)LCOc6(or 8)r3(or 6), depending on the presence or absence of Pd, with “c” and “r” representing “precalcined” and “prereduced,” respectively, and 3 (= 300 °C), 6 (= 600 °C), and 8 (= 800 °C) indicating the temperature of the treatment. For example, PdLCOc8r3 represents 0.5 wt% Pd/LaCoO<sub>3</sub> calcined at 800 °C, followed by reduction at 300 °C.

Catalyst stability versus time on stream was measured at the temperature of maximum NO conversion ( $T_{\text{max}}$ ) for 100 h under flowing reaction mixture, increasing  $T$  from 50 °C to  $T_{\text{max}}$  at a rate of 2 °C/min. GC analysis was done every hour for the first 12 h and then every 2 h from 12 to 26 h, every 4 h from 26 to 60 h, and every 10 h from 60 to 100 h.

Thermal resistance of the catalyst was measured by carrying out the reaction on samples prereduced at 300 °C, then cooled

in the flowing reaction mixture and repeating the temperature ramp to measure the residual NO conversion. In addition, the catalyst demonstrating the best performance was submitted to three activation–deactivation cycles. The sample was reoxidized by the reaction gas mixture (containing excess O<sub>2</sub>) when ramping to 320 °C, followed by reduction at 300 °C in flowing 10% H<sub>2</sub>/He.

### 2.3. Transient experiments

Temperature-programmed experiments were performed in the same setup used for the catalytic activity tests. The fresh catalyst bed (ca. 0.15 g, 0.20–0.30 mm particle size, diluted 1:4 by weight with quartz powder of the same particle size) was pretreated in 10% O<sub>2</sub>/He (20 cm<sup>3</sup>/min) at either 600 or 800 °C. The Pd-containing catalyst was prereduced in 10% H<sub>2</sub>/He (20 cm<sup>3</sup>/min) at 300 °C for 30 min, followed by reoxidation at 160 °C for 30 min in 20% O<sub>2</sub>/He. In this way, the reduced support was reoxidized to LaCoO<sub>3</sub>, whereas the surface Pd and Co particles retain their bulk metallic state [32]. This step was done to favor adsorption rather than reaction of adsorbed NO with the reduced support. The outlet gas composition was monitored by QMS. The  $m/z$  mass fragments 2, 12, 14, 18, 28, 30, 32, 44, and 46, corresponding to H<sub>2</sub>, C, N, H<sub>2</sub>O, N<sub>2</sub>, NO, O<sub>2</sub>, N<sub>2</sub>O, and NO<sub>2</sub>, were monitored. In particular, N<sub>2</sub> and N<sub>2</sub>O were distinguished from CO and CO<sub>2</sub> by the trend of  $m/z = 12$ . Indeed, the fact that the latter signal remained unperturbed during the experiment indicates that no C-containing species were formed or consumed.

The sequence of steps for the NO-TPD and TPSR experiments is summarized in Table 1. In all cases, the overall gas flow rate was 30 mL/min and the temperature ramp was 5 °C/min.

### 2.4. In situ fluorescence XANES and EXAFS during NO/H<sub>2</sub>/O<sub>2</sub> reaction

XANES and EXAFS data were collected at the Norwegian–Swiss beamline (SNBL, BM01B) of the European Synchrotron Radiation Facility, ESRF, Grenoble, France. The spectra were obtained using a specially designed *in situ* cell [33], loaded with 0.180 g of sample powder, pelletized, crushed, and sieved to 50–100 μm. For *in situ* oxidation, reduction, and reaction, 21% O<sub>2</sub>/He, 5% H<sub>2</sub>/He, and 0.25% NO/1% H<sub>2</sub>/5% O<sub>2</sub>/He (ramp 2 °C/min), respectively, were fed to the reactor cell. The evolving products during TPR/TPO were monitored by a Balzers Thermostat QMS instrument.

The spectra around the Pd K-edge (24.350 keV) were recorded in fluorescence mode using a 13-element Ge-solid state detector (Canberra). For this purpose, the fluorescence signals from the 13 detector elements were preamplified and then fed into the XIA digital pulse processing electronics (DXP 2X). The Pd  $K\alpha$ -fluorescence regions were selected and calibrated on the basis of a full spectrum for each channel, collected before the measured scans. To minimize the fluorescence from the matrix, aluminum and chromium filters were added. The resulting SCA data were added up manually after each measurement,

Table 1  
Sequence of steps of the different temperature-programmed experiments

Experiment	Sequence of steps
NO-TPD	2.5% NO/He (30 °C; 30 min) → He (30 °C; 30 min) → TPD in He
TPSR-1	2.5% NO/He (30 °C; 30 min) → He (30 °C; 30 min) → TPSR in 4% H <sub>2</sub> /10% O <sub>2</sub> /He
TPSR-2	1% NO/20% O <sub>2</sub> /He (150 °C; 30 min) → cooling in the same flowing gas mixture to 30 °C → He (30 °C; 30 min) → TPSR in 4% H <sub>2</sub> /10% O <sub>2</sub> /He
TPSR-3	1% NO/20% O <sub>2</sub> /He (150 °C; 30 min) → cooling in the same flowing gas mixture to 30 °C → He (30 °C; 30 min) → TPSR in 10% H <sub>2</sub> /He
TPSR-4	On the sample after the TPSR2 → cooling in 4% H <sub>2</sub> /10% O <sub>2</sub> /He to 30 °C → He (30 °C; 30 min) → TPSR in 10% H <sub>2</sub> /He

Note. Common conditions: 0.150 g of catalyst; 30 mL/min total gas flow rate; 5 °C/min temperature ramp.

and the spectra were background-corrected and normalized using WINXAS 3.1 software [34]. Data fitting was performed in the  $R$  space on the Fourier-transformed  $k^3$ -weighted EXAFS functions (Fourier transform in the range of 3.5–14 Å,  $S_0^2 = 0.7$ ). Theoretical scattering amplitudes and phase shifts of the Pd–Pd shell and the Pd–O shell (only first shell) were calculated using the FEFF code [35].

### 3. Results

#### 3.1. Catalytic activity

##### 3.1.1. Effect of calcination temperature

The plots of NO conversion ( $X_{\text{NO}}$ ), selectivity to N<sub>2</sub> ( $S_{\text{N}_2}$ ), and H<sub>2</sub> conversion ( $X_{\text{H}_2}$ ) versus temperature over Pd-modified and -unmodified FP-LaCoO<sub>3</sub>, are reported in Fig. 1. LCOc6 showed only oxidative activity of NO to NO<sub>2</sub> (reaction 3) in the 160–450 °C range, with a maximum  $X_{\text{NO}}$  of 86% at 310 °C. Preannealing at higher temperature (sample LCOc8) provoked a partial catalyst deactivation, with a maximum  $X_{\text{NO}}$  of 53% at 380 °C. However, a small reductive activity to N<sub>2</sub> (reaction (1)) was detected in this range, with a maximum  $S_{\text{N}_2}$  of 8% at 290 °C ( $X_{\text{NO}} = 15.4\%$ ). In contrast, the Pd-containing perovskite reduced at 300 °C displayed two  $X_{\text{NO}}$  maxima, one at 100–250 °C, due to the reduction of NO to N<sub>2</sub> and N<sub>2</sub>O (reactions (1) and (2)), and the second one at higher temperature, due to the oxidation activity of the perovskite support. In particular, PdLCOc6r3 was less active for the reduction of NO to N<sub>2</sub> ( $T_{\text{max}} = 210$  °C,  $X_{\text{NO}} = 67\%$ ,  $S_{\text{N}_2} = 62\%$ ) than PdLCOc8r3 ( $T_{\text{max}} = 150$  °C,  $X_{\text{NO}} = 100\%$ ,  $S_{\text{N}_2} = 67\%$ ). Thus, a higher calcination temperature had a beneficial effect on the reduction activity but a detrimental effect on the oxidation activity. Both the PdLCOc6r3 and PdLCOc8r3 catalysts attained the highest  $S_{\text{N}_2}$  between 200 and 260 °C, just before the start of oxidation activity to NO<sub>2</sub>, whereas H<sub>2</sub> ( $X_{\text{H}_2}$ ) and NO ( $X_{\text{NO}}$ ) conversions started at the same temperature. Except for LCOc8, in all other cases  $X_{\text{H}_2}$  attained 100% at  $T > 350$  °C, and PdLCOc8r3 allowed full conversion of H<sub>2</sub> already at 150–210 °C.

##### 3.1.2. Effect of reduction temperature

Fig. 2 shows that the FP-made PdLCO, preannealed at 800 °C, showed a first  $X_{\text{NO}}$  maximum (21%) at 250 °C ( $S_{\text{N}_2} = 86\%$ ). This activity was not observed for LCOc8 and is similar to that reported by Engelmann-Pirez et al. [15]. Reduction at 300 °C in flowing 10% H<sub>2</sub>/He led to improved NO reduction according to reaction (1) (*vide supra*), whereas the catalyst reduced at 600 °C (PdLCOc8r6) displayed  $X_{\text{NO}} = 100\%$  for

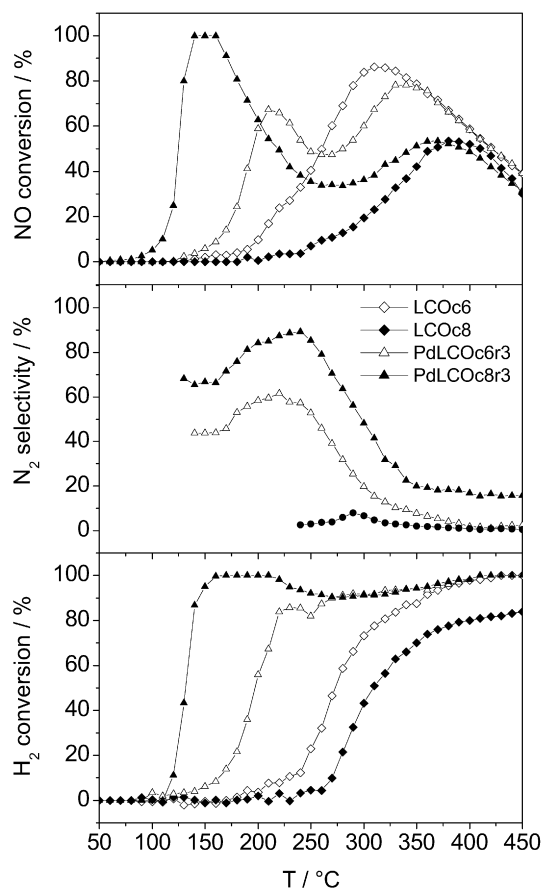


Fig. 1. Effect of precalcination temperature on catalytic activity for the NO/H<sub>2</sub>/O<sub>2</sub> reaction of LCO (triangles) and PdLCO (diamonds). Calcination temperature: 600 °C (empty dots) and 800 °C (full dots). The Pd-containing catalysts were reduced at 300 °C before the catalytic test. Reaction conditions: 0.15 g of catalyst; 0.25% NO/1% H<sub>2</sub>/5% O<sub>2</sub>/He (100 mL/min); 2 °C/min temperature ramp.

a wider temperature range (140–180 °C,  $S_{\text{N}_2} = 77\%$ ). Furthermore, in both cases, the FP-made PdLCO had superior catalytic activity compared with the same catalyst prepared by impregnation (impPdLCOc5r3). Indeed, the latter never reached full NO conversion under the reaction conditions used here ( $T_{\text{max}} = 180$  °C,  $X_{\text{NO}} = 78\%$ ,  $S_{\text{N}_2} = 67\%$ ). In contrast, the impregnated catalyst was the most active for H<sub>2</sub> conversion ( $X_{\text{H}_2}$ ) in the 200–450 °C temperature range. Indeed, whereas impPdLCOc5r3 maintained a 100%  $X_{\text{H}_2}$ ,  $X_{\text{H}_2}$  decreased to 90% for PdLCOc8r3 and to 56% for PdLCOc8r6. Because  $X_{\text{NO}}$  was always lower with impPdLCOc5r3 than with the prerduced FP-made catalyst throughout the entire temperature range, we can

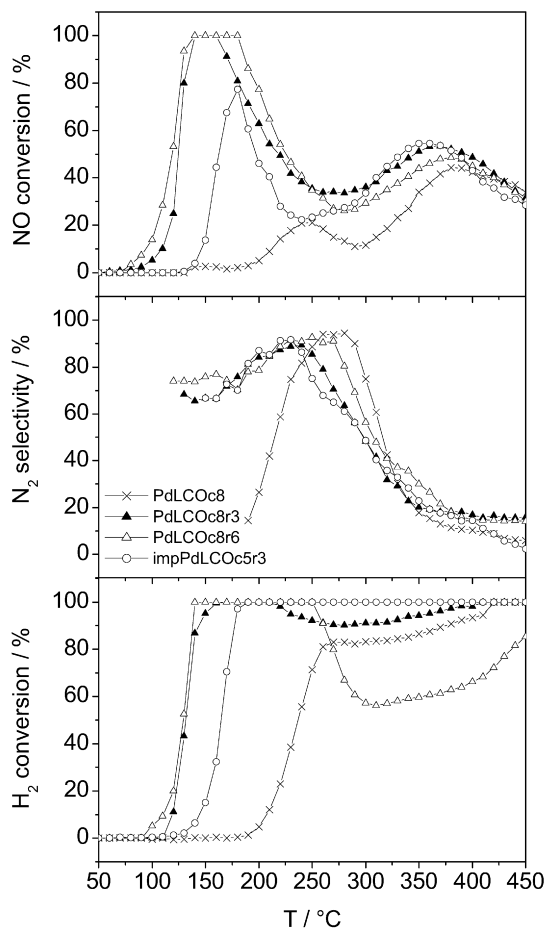


Fig. 2. Effect of prereduction temperature on catalytic activity for the NO/H<sub>2</sub>/O<sub>2</sub> reaction of PdLCO (precalcined at 800 °C). (x) PdLCOc8 (not pre-reduced); (▲) PdLCOc8r3 (reduced at 300 °C); (△) PdLCOc8r6 (reduced at 600 °C); (○) impPdLCOc5r3 (perovskite support precalcined at 800 °C before Pd impregnation). Reaction conditions: 0.15 g of catalyst; 0.25% NO/1% H<sub>2</sub>/5% O<sub>2</sub>/He (100 mL/min); 2 °C/min temperature ramp.

conclude that with impPLCOc5r3, hydrogen reacted preferably with O<sub>2</sub> to form water, rather than with NO to form N<sub>2</sub>, thus decreasing the catalytic activity for NO reduction.

### 3.1.3. Time on stream and thermal resistance of catalyst

The stability of PdLCOc8r3 (Fig. 3) and PdLCOc8r6 (not shown) was tested under steady-state reaction conditions at 160 °C ( $T_{max}$ ). Both catalysts displayed full NO conversion after 100 h on stream. Furthermore, while remaining constant at 78% for PdLCOc8r6,  $S_{N_2}$  increased from 68% to 78% for PdLCOc8r3 during the first 10 h and then attained the performance of PdLCOc8r6. In addition, the conversions of H<sub>2</sub> and O<sub>2</sub> were stable at 100 and 10%, respectively. In contrast, in the case of impPdLCOc5r3 (Fig. 3),  $X_{NO}$  decreased from 78 to 55% at 180 °C ( $T_{max}$ ) during the first 10 h and then stabilized at this value for the remaining 90 h on stream. The trends for  $X_{H_2}$ ,  $X_{O_2}$ , and  $S_{N_2}$  were similar to those exhibited by PdLCOc8r3.

Fig. 2 shows that either PdLCOc8r3 or PdLCOc8r6 exhibited a saddle in the  $X_{NO}$  in the 200–320 °C range, where the reduction activity (reactions (1) and (2)) dropped and the ox-

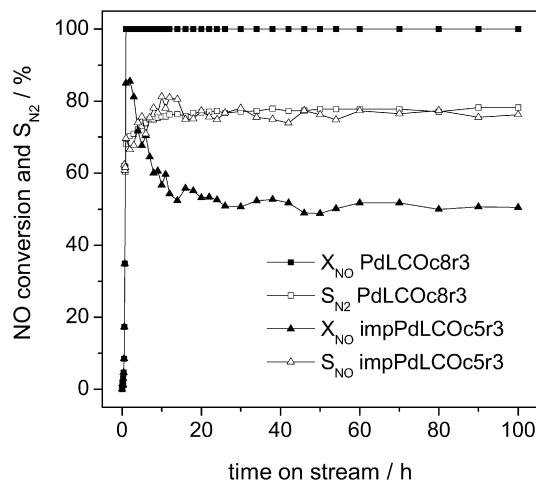


Fig. 3. Catalyst resistance vs time-on-stream at the temperature of max NO conversion: 160 °C (squares) for PdLCOc8r3; 180 °C (triangles) for impPdLCOc5r3. Full dots: NO% conversion, empty dots: selectivity to N<sub>2</sub>.

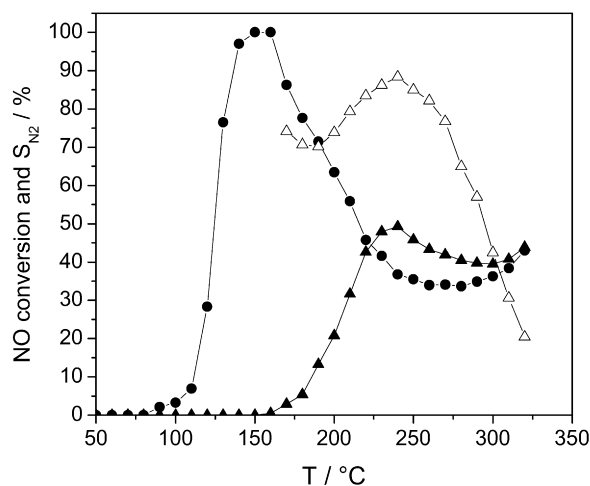


Fig. 4. Catalytic activity of PdLCOc8r3 after three activation cycles in flowing 10% H<sub>2</sub>/He and deactivation in reaction gas flowing mixture (NO/H<sub>2</sub>/O<sub>2</sub>/He) up to 320 °C. (●) NO% conversion after the third reactivation cycle; (▲) residual NO% conversion after the third thermal deactivation; (△) selectivity to N<sub>2</sub> after the third deactivation cycle.

idation activity (reactions (3) and (4)) became predominant. To check whether such a drop in catalytic activity was due to a thermal phenomenon or to catalyst deactivation, a thermal resistance test was performed on PdLCOc8r3 (Fig. 4), as reported in Section 2. This test simulates a possible catalyst overheating from the  $T_{max}$  of 160 °C. The data show that the catalyst underwent a partial deactivation, with the first maximum shifted to 240 °C ( $X_{NO} = 48\%$ ,  $S_{N_2} = 88\%$ ). A similar result was obtained when PdLCOc8r3 was overheated up to 500 °C; however, the catalyst was fully reactivated in flowing 10% H<sub>2</sub>/He at 300 °C, even after several cycles of thermal deactivation. Fig. 4 shows the activity of PdLCOc8r3 after three cycles of reactivation and the residual NO conversion after the subsequent thermal deactivation at 320 °C under a flowing reaction mixture.

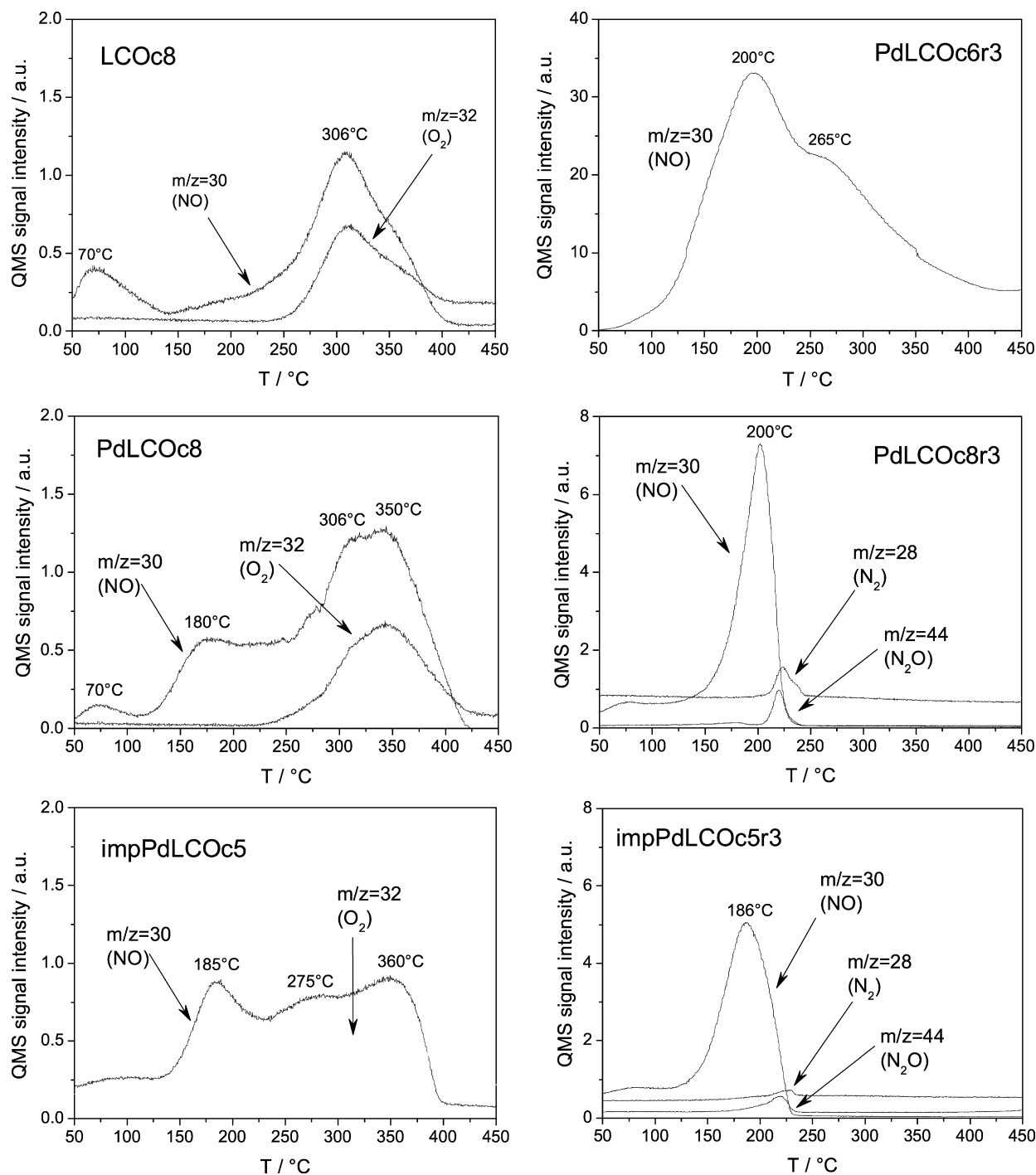


Fig. 5. TPD-NO spectra of NO preadsorbed at 30 °C and species released in the 50–450 °C range with heating rate = 5 °C/min.

### 3.2. TPD of NO

Fig. 5 shows the thermal desorption patterns of some selected samples at 50–450 °C after NO chemisorption at 30 °C followed by TPD in flowing He with a temperature ramp rate of 5 °C/min. For LCOc8, PdLCOc8, and impPdLCOc5, three NO desorption windows can be recognized: at 50–100 °C, due to desorption of physisorbed NO; at 125–250 °C, due to desorption of nitrosyls chemisorbed on surface metallic Co and Pd atoms or cations [36,37]; and at 225–425 °C, with two max-

ima at 306 °C and at 350 °C, due to decomposition of surface nitrites ( $M-O-N=O \rightarrow M + NO + \frac{1}{2}O_2$ ) and mono or bidentate nitrates ( $M-O-NO_2$  [or  $M-O-(NO)-O-M$ ]  $\rightarrow M + NO + O_2$ ) [38,39], formed by interaction with surface oxygen anions ( $\alpha$ -oxygen). Indeed, in the last window,  $O_2$  desorption also was detected, along with NO. Only nitrite structures have been associated with  $La^{3+}$  ions [38], whereas nitrosyl and nitrate species typically form on surface Co or Pd-containing species [36,37].

Some important differences arise from the comparison of the thermal desorption patterns of the three samples. In particular,

the Pd-containing catalysts, PdLCOc8 and impPdLCOc5, exhibited a more intense NO desorption in the 125–225 °C range ( $T_{\max} = 185$  °C). The origin of this NO evolution can be reasonably attributed to nitrosyls adsorbed on segregated  $\text{Co}_3\text{O}_4$  and PdO. Furthermore, impPdLCOc5 displayed more pronounced  $\text{NO} + \text{O}_2$  evolution at 270 °C, likely due to decomposition of nitrates formed on the more abundant PdO surface particles present on the impregnated catalyst.

With the Pd-containing catalysts, noticeable changes in the NO-TPD patterns occurred after reduction at 300 °C in flowing 10%  $\text{H}_2/\text{He}$ , followed by bulk reoxidation of the support to the perovskite at 160 °C in flowing 20%  $\text{O}_2/\text{He}$ . Both PdLCOc8r3 and impPdLCOc5r3 exhibited a single NO desorption peak at 125–225 °C ( $T_{\max} = 185$  °C for impPdLCOc5r3 and 200 °C for PdLCOc8r3), followed by a weak evolution of  $\text{N}_2$  and  $\text{N}_2\text{O}$  at around 225 °C. The formation of  $\text{N}_2$  and  $\text{N}_2\text{O}$  is due to the coupling of two N adatoms, produced by dissociative NO adsorption, and to the reaction of an N adatom with another NO molecule, respectively. Similar patterns were reported by de Wolf and Nieuwenhuys [36] for NO adsorbed at 27 °C over a Pd(111) single-crystal surface. The peak at 200 °C can be attributed to desorption of nitrosyls from Pd particles, although a contribution of nitrosyls desorbed from the perovskite surface cannot be excluded. Because neither NO nor  $\text{O}_2$  evolution was detected in the temperature range of nitrite and nitrate decomposition, we can conclude that the reoxidation at 160 °C was not sufficient to restore the surface oxygen anion sites ( $\alpha$ -oxygen) of PdLCOc8, over which gaseous NO interacts to form the surface nitrates and nitrites. However, the formation of other more strongly adsorbed NO species, neither desorbing nor decomposing within the temperature range considered here, cannot be excluded.

Moreover, the NO peak area, proportional to the amount of desorbed NO, obtained with impPdLCOc5r3, was 10% smaller than that obtained with PdLCOc8r3. This result could be correlated to a higher Pd dispersion in the FP-made catalyst compared with the impregnated catalyst.

Finally, in the NO-TPD patterns of PdLCOc6r3, along with the desorption peak at 200 °C, also observed on PdLCOc8r3, a second contribution appeared at 265 °C. This second peak might be attributed to NO adsorbed on the support surface. The latter could be either lacking after calcination at 800 °C, mainly due to particle sintering, or desorbing at lower temperature, thus overlapping to the NO desorbed from Pd. Moreover, the amount of desorbed NO was ca. 4 times greater than that desorbed from PdLCOc8r3, clearly due to the higher specific surface area of the sample calcined at 600 °C (20 vs 8  $\text{m}^2/\text{g}$ ).

### 3.3. TPSR

In the previous section, we found that NO adsorbed at 30 °C on surface Pd particles on PdLCOc8r3 and desorbed under He flow at around 200 °C. To establish the role of this NO species in the catalytic activity and thus in the reaction mechanism, we tested its stability under a  $\text{H}_2/\text{O}_2/\text{He}$  flow while increasing the temperature to 300 °C (TPSR-1; Table 1). The QMS signal trends, similar to those obtained on impPdLCOc5r3, are

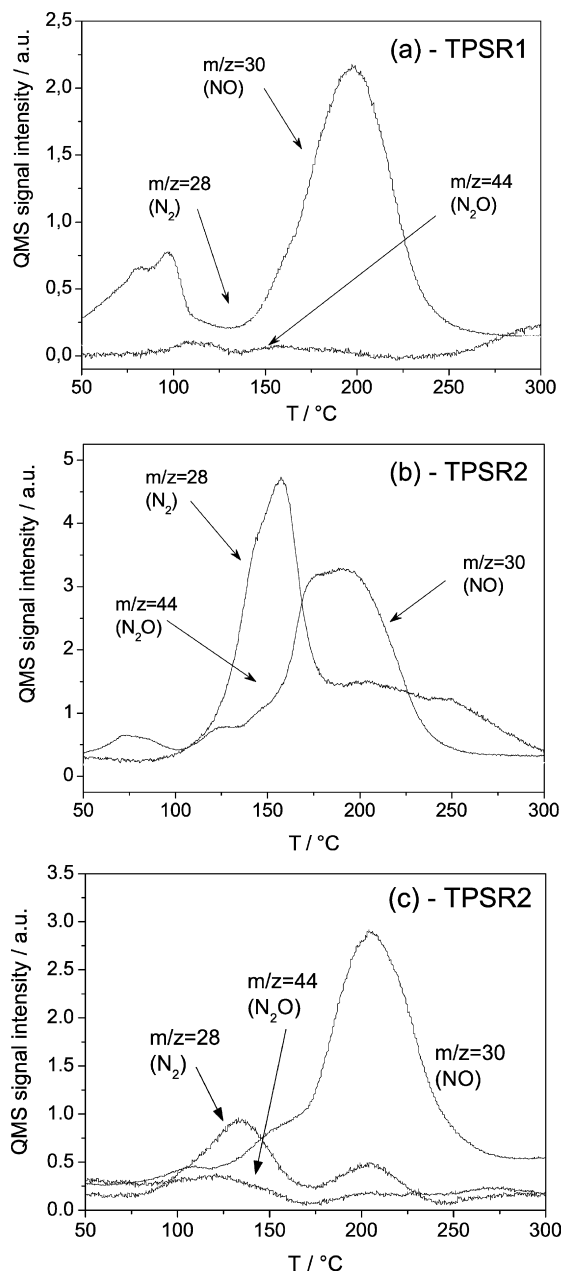


Fig. 6. QMS analysis of the species evolved during the TPSR-1 (a) and TPSR-2 (b) experiments over PdLCOc8r3 and TPSR2 (c) over impPdLCOc5r3.

shown in Fig. 6a. The main evolved species was again NO at around 200 °C, whereas a weak evolution of  $\text{N}_2$  and  $\text{N}_2\text{O}$  occurred at 100–200 °C. Thus, NO adsorbed at 30 °C on Pd contributed only slightly to the reaction. Different and more interesting results were achieved when NO was co-adsorbed with  $\text{O}_2$  at 150 °C (TPSR-2; Fig. 6b). Indeed, in this case, the more intense signal was that of  $\text{N}_2$ , evolved mainly in two different zones: 100–180 °C, with a maximum at 160 °C, which also corresponds to the temperature of maximum  $X_{\text{NO}}$  (Fig. 2), and at 180–300 °C, with a maximum at 210 °C. In contrast,  $\text{N}_2\text{O}$  showed a QMS signal intensity lower than that of  $\text{N}_2$  and evolved only in the former temperature range. These results are in line with the experimental  $S_{\text{N}_2}$  trend at 100–300 °C observed on PdLCOc8r3 (Fig. 2). Indeed, at 180–300 °C, where no evo-

lution of  $\text{N}_2\text{O}$  was detected,  $S_{\text{N}_2}$  increased to 90%. Finally, the signal corresponding to NO displayed a peak centered at 200 °C. Thus no relevant change in the NO desorption curve was noticed with respect to the TPSR-1 experiment.

The TPSR-2 experiment conducted on impPdLCOc5r3 is reported in Fig. 6c. The amount of evolved  $\text{N}_2$  was clearly lower than that in PdLCOc8r3, and, in particular, the contribution at 160 °C was completely absent. This result represents a significant difference with respect to PdLCOc8r3 and suggests the presence of a greater amount of active species, and thus active sites, which would explain the better catalytic performance of the FP-made catalyst.

A third TPSR experiment (TPSR-3) was conducted to investigate the stability of the N-containing species produced after adsorption of  $\text{NO} + \text{O}_2$  at 150 °C under a 10%  $\text{H}_2/\text{He}$  flow, that is, in an oxygen-free atmosphere. The results are reported in Fig. 7a. The area under the  $\text{N}_2$  signal was three times larger than that obtained in TPSR-2. Thus, in the absence of  $\text{O}_2$ , more  $\text{N}_2$  evolved from the catalyst. Moreover, no  $\text{N}_2\text{O}$  was detected, whereas the formation of ammonia cannot be excluded at 100–150 °C. In fact, the  $m/z = 17$  signal corresponds to the sum of both the parent  $\text{NH}_3$  and the  $\text{OH}^-$  fragment of water, which amounts to the 23% of the main  $m/z = 18$  signal. The weighted subtraction of the 18- and 17- $m/z$  signals should give, as a residual, the contribution due to ammonia only; the result was a peak centered at 120 °C. Fig. 7a also shows the deconvolution of the  $\text{N}_2$  signal, which led to four contributions at 120, 145, 170, and 210 °C.

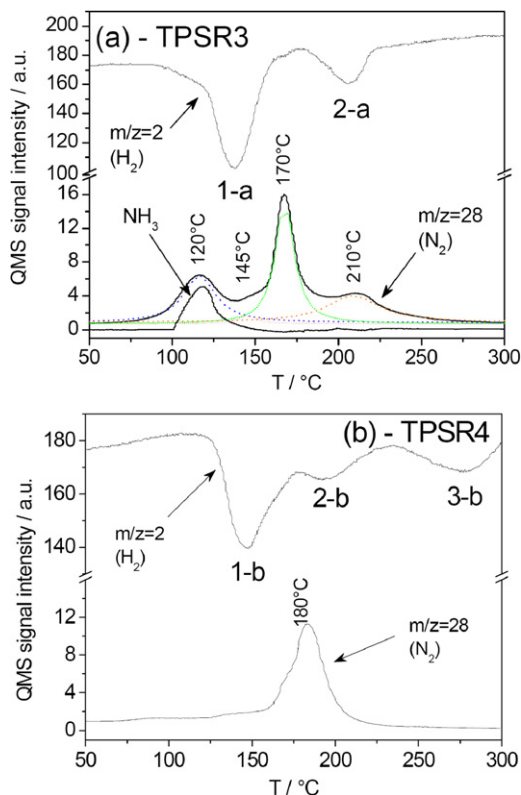


Fig. 7. QMS analysis of the species evolved during the TPSR-3 (a) and TPSR-4 (b) experiments according to Table 1.

Fig. 7b shows the results of a TPSR experiment in 10%  $\text{H}_2/\text{He}$  (TPSR-4) on PdLCOc8r3 after TPSR-2. In this case, the reduction of the residual N-containing species was obtained. But the latter do not participate in the reaction, remaining as spectator species [19,20] accumulating onto the catalyst surface, stabilized by the presence of oxygen. The only remaining contribution was that at 180 °C. Note that no ammonia was detected in this case. Finally, the uptake of  $\text{H}_2$  exhibited in these last two experiments was due mainly to the reduction of the catalyst itself [32], particularly of  $\text{LaCoO}_3$  to  $\text{La}_3\text{Co}_3\text{O}_8$  (steps 1a and 1b in Fig. 7) and of  $\text{La}_3\text{Co}_3\text{O}_8$  to  $\text{La}_2\text{Co}_2\text{O}_5$  (steps 2a and 3b). Furthermore, step 2b, which was absent during TPSR-3, was due to the reduction of cobalt oxide particles. Indeed, the reduction process at 300 °C produced metallic Co particles, stable in oxygen-rich atmosphere at 160 °C [32]. At higher temperature, they reoxidized, as occurred after TPSR-2.

### 3.4. In situ XANES and EXAFS during the $\text{NO}/\text{H}_2/\text{O}_2$ reaction

In situ XANES measurements on PdLCOc8r3 during the  $\text{NO}/\text{H}_2/\text{O}_2$  reaction (Fig. 8a) showed that at 160 °C [i.e., the temperature of maximum NO conversion (Fig. 2)], Pd was still prevalent in the reduced state, whereas almost full oxidation occurred at 500 °C. In particular, the trend of the fraction of  $\text{Pd}^{2+}$  at a given temperature (Fig. 8b), obtained by linear combination analysis (LCA) of the XANES spectra recorded at that temperature with those of PdLCOc8 (fully oxidized Pd) and of PdLCOc8r3 (fully reduced Pd), revealed that the reoxidation of Pd occurred in three steps at 25–500 °C. Under the reaction mixture, Pd was stable up to 150 °C, followed by mild oxidation (ca. 20%) at 160–200 °C, due in part to surface reoxidation and reoxidation of the smallest Pd particles. No further oxidation occurred in the 200–300 °C range, whereas rapid reoxidation was recorded from 300 °C on. In contrast, PdLCOc8r6 displayed different behavior, because  $\text{Pd}^0$  was found to be more stable under the reaction gas mixture. Indeed, LCA showed that reoxidation occurred only over 300 °C. Moreover, in the 25–270 °C range, LCA did not fit the experimental data when the XANES spectrum of PdLCOc8r3 was taken as reference for  $\text{Pd}^0$ , whereas the spectrum of PdLCOc8r6 did fit, due to the presence of the Pd–Co alloy. The opposite occurred with LCA of the spectra recorded above 270 °C, where fitting was possible using the spectrum of PdLCOc8r3; therefore, the Pd–Co alloy was stable up to 270 °C.

The FT-EXAFS spectra of PdLCOc8r3 during reaction at 160 and 500 °C are presented in Fig. 9. In the former case, although a weak contribution at 1.6 Å was observed due to the oxygen first-neighbor shell, indicating a partial oxidation, the main contribution was still at 2.5 Å, typical of Pd–Pd distance of metallic Pd (compare with FT-EXAFS of Pd foil in Fig. 9). Hardly any contribution was found at the Pd–La distance (3.2 Å), indicating that no Pd incorporation in the perovskite framework occurred at 160 °C. On the other hand, the spectrum of PdLCOc8r3 (Fig. 9b) measured during reaction at 500 °C demonstrated clear reoxidation of the sample with an increase of the feature at 1.7 Å (Pd–O distance). Peak deconvolution in the 2–4 Å range showed the presence of three

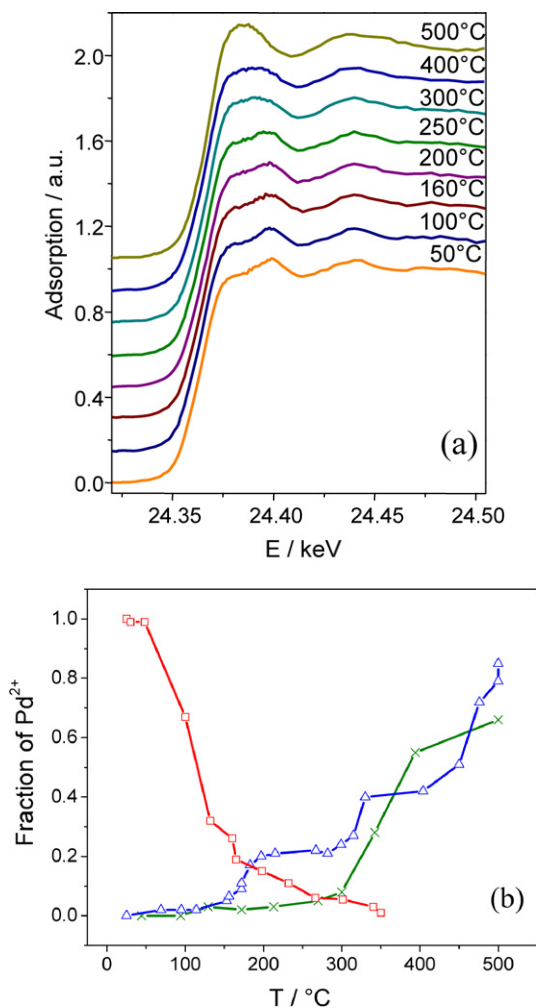


Fig. 8. (a) *In situ* fluorescence XANES at the Pd K-edge during NO/H<sub>2</sub>/O<sub>2</sub> reaction over PdLCOc8r3 at different temperatures. (b) Fraction of Pd<sup>2+</sup> obtained by linear combination analysis of the *in situ* fluorescence XANES spectra during reduction of PdLCOc8 in 10% H<sub>2</sub>/He up to 350 °C (□); NO/H<sub>2</sub>/O<sub>2</sub> reaction over PdLCOc8r3 (△) and over PdLCOc8r6 (×).

contributions centered at 2.5, 2.9, and 3.3 Å, which were ascribed to the Pd–Pd distance in metallic Pd, the Pd–Pd distance in PdO, and the Pd–La distance of Pd placed at the B site of the ABO<sub>3</sub> perovskite framework, respectively. Therefore, after exposure at 500 °C under the reaction gas mixture, only a small fraction of Pd was still reduced (ca. 10%, Fig. 8b), whereas the remainder was oxidized, in part as surface PdO and in part as Pd<sup>2+</sup> dissolved into the perovskite. This demonstrates that Pd can segregate on the surface during the reduction process and move back into the perovskite bulk when exposed to oxygen-rich atmosphere at relatively high temperature. Similar behavior was reported for other Pd-doped perovskites [16].

#### 4. Discussion

The present results show how the temperature of precalcination and successive reduction decisively affect the catalytic performance of the FP-made catalyst, as a consequence of the different structural modifications during these processes, namely sintering, Co<sub>3</sub>O<sub>4</sub> and Pd segregation, a change in the

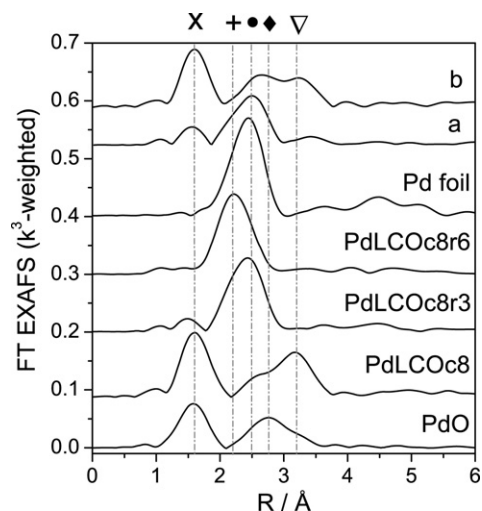


Fig. 9. Radial distribution function (FT-EXAFS spectra at the Pd K-edge) around Pd of some selected samples. PdLCOc8r3 during NO/H<sub>2</sub>/O<sub>2</sub> reaction at 160 °C (a) and after 500 °C (b). Interatomic distances: (×) Pd–O; (+) Pd–Co; (●) Pd–Pd in Pd<sup>0</sup> particles; (◆) Pd–Pd in PdO particles; (▽) Pd–La.

Pd oxidation state, and formation of the Pd–Co alloy [32]. The highest catalytic activity in H<sub>2</sub>-SCR was attained after precalcination at 800 °C, followed by reduction, over both PdLCOc8r3 and PdLCOc8r6. Furthermore, the FP-made catalyst proved superior to the same material created by the conventional impregnation method (impPdLCOc5r3), in terms of conversion of NO ( $X_{NO}$ ; Fig. 2) and lifetime (Fig. 3). Momentarily neglecting PdLCOc8r6, which has a completely different catalyst formulation (Pd–Co alloy on CoO<sub>x</sub>–La<sub>2</sub>O<sub>3</sub>), what really differentiates PdLCOc8r3 from PdLCOc6r3 and impPdLCOc5r3 is the presence of cobalt metal nanoparticles at the catalyst surface. Pd particle size seems not to be a crucial property in the NO/H<sub>2</sub>/O<sub>2</sub> reaction over this catalyst. Indeed, PdLCOc6r3 displayed lower catalytic performance, with the maximum  $X_{NO}$  lower and shifted to higher temperature, despite the fact that it had Pd particles smaller than impPdLCOc5r3 but similar to PdLCOc8r3 [32]. This might indicate that dissociative hydrogen adsorption over Pd is not the rate-determining step.

The TPSR-2 experiment (Fig. 6b) clearly showed that the N-containing active species form on NO and O<sub>2</sub> co-adsorption at  $T_{max} = 160$  °C, whereas the TPSR-1 experiment (Fig. 6a) showed that NO preadsorbed at 30 °C on Pd reacted only slightly with H<sub>2</sub> in the presence of O<sub>2</sub>. Moreover, although the TPSR-1 results collected on PdLCOc8r3 and on impPdLCOc5r3 were similar, involving the same NO adsorbed species on Pd, the TPSR-2 data were considerably different (Fig. 6). According to Costa and Efsthathiou [20], two structurally different and adjacent active N-species lie on the support, namely bidentate nitrates and nitrosyls, that can be efficiently reduced to N<sub>2</sub> and water by spillover of hydrogen dissociatively adsorbed on Pd particles [6]. Because nitrates do not form on La<sup>3+</sup> [38], although NO/O<sub>2</sub> co-adsorption over Co<sup>2+</sup> sites is known to lead to the formation of surface nitrates [40], we can conclude that one of the two active N-species (the bidentate nitrates) forms over Co sites. Therefore, we suggest that the enhanced catalytic activity of PdLCOc8r3 compared with

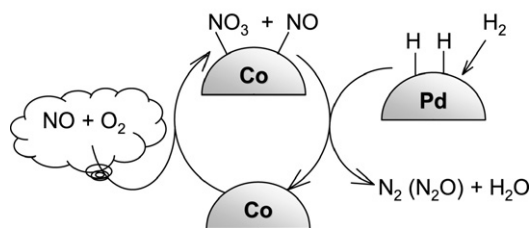


Fig. 10. Simplified scheme of the cooperative reaction mechanism occurring in the 125–175 °C temperature range over PdLCOc8r3.

impPdLCOc5r3 is due to the surface Co metal particles acting as more efficient NO/O<sub>2</sub> co-adsorption sites compared with the bare perovskite surface. This hypothesis is supported by the TPSR-2 experiment (Fig. 6), which showed a greater amount of active species present on PdLCOc8r3 than on impPdLCOc5r3, where no surface Co particles were seen (*vide supra*). Therefore, the reaction occurring at 160 °C on PdLCOc8r3 could follow a cooperative mechanism, going through the oxidation to Co<sup>2+</sup> of Co metal particle surface by co-adsorption of NO and O<sub>2</sub> to give cobalt nitrates. The latter then readily react with nitrosyls and subsequently reduce to N<sub>2</sub>, N<sub>2</sub>O, and water by the hydrogen spillover from Pd, thus restoring the Co metal site (scheme of Fig. 10). Further work is now in progress, through *in situ* DRIFT analysis, to better elucidate this aspect. Fig. 11 presents a STEM image of a possible active site on PdLCOc8r3, showing the proximity of Co and Pd particles on LaCoO<sub>3</sub>. As mentioned in the accompanying paper [32], surface Co particles have not been detected by STEM analysis on either impPdLCOc5r3 or PdLCOc6r3.

When the temperature was increased to 300 °C, the Co<sup>0</sup> particles were irreversibly oxidized to Co<sub>3</sub>O<sub>4</sub>, thus suppressing the mechanistic route proposed here. The oxidation of CoO to Co<sub>3</sub>O<sub>4</sub> also has been found to be detrimental for the NO/C<sub>3</sub>H<sub>6</sub>/O<sub>2</sub> reaction over CoO<sub>x</sub>/ZrO<sub>2</sub> [37]. Moreover, *in situ* XANES measurements demonstrated that ca. 20% of Pd reoxidized at 160–300 °C (Fig. 8b). These two aspects are in line with the partial catalyst deactivation observed after heating at 300 °C under the reaction gas mixture (thermal resistance tests of Fig. 4). Successive reduction at 300 °C reactivated the catalyst by restoring the Co and Pd metal particles. The residual NO reduction activity at 180–280 °C seems to be the same as that found over PdLCOc8 (Fig. 2) and can be reasonably attributed to a different reaction mechanism. The latter implies the dissociative NO adsorption over Pd particles, forming N adatoms, which can either couple to form N<sub>2</sub> or react with another NO molecule to form N<sub>2</sub>O (*vide supra*). Oxygen adatoms are removed by reaction with H adatoms to form water.

PdLCOc8r6 proved to be the most active catalyst, displaying full NO conversion in a wider temperature range (140–180 °C), with greater selectivity to N<sub>2</sub> at 160 °C than for the other catalysts (77% vs 67%). The improved performance can be attributed to formation of the Pd–Co alloy, for two reasons: The alloy is more stable to reoxidation than separated Pd and Co metal particles, as revealed by XANES analysis (Fig. 8a), and the proposed cooperative reaction mechanism (Fig. 10) can occur more efficiently on the alloy due to the

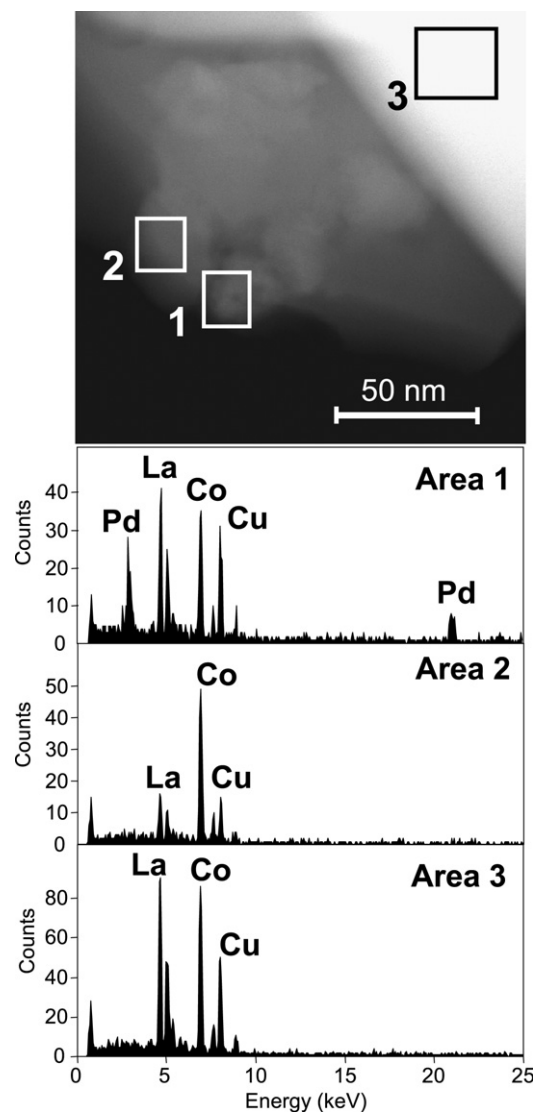


Fig. 11. HAADF-STEM images and EDX spectra of a possible reaction site of PdLCOc8r3, showing the proximity of surface Pd (area 1) and Co (area 2) particles on LaCoO<sub>3</sub> (area 3). The Cu peak is caused by the sample-supporting grid.

intimate contact between Pd and Co atoms. As we report in the accompanying paper [32], PdLCOc8r6 displayed the highest coordination number ( $11.8 \pm 1$ , calculated by EXAFS data fitting; Table 2), indicating that the Pd-containing particles were remarkably large. But also in this case, this parameter seemed to not affect the catalytic performance; on the other hand, larger particles are less prone to reoxidation. Although the alloy was stable up to 300 °C,  $X_{\text{NO}}$  started to decrease already at 180 °C, whereas  $X_{\text{H}_2}$  remained unchanged at 100% up to 250 °C, and  $X_{\text{O}_2}$  increased slightly (from 10 to 12%). This suggests that over 180 °C, the direct reaction of H<sub>2</sub> with O<sub>2</sub> to give H<sub>2</sub>O became predominant, whereas the slight increase of  $X_{\text{O}_2}$  was due to oxidation of CoO<sub>x</sub> to Co<sub>3</sub>O<sub>4</sub>.

Finally, a significant result came from *in situ* EXAFS analysis on PdLCOc8r3 after reaction at 500 °C (Fig. 9), demonstrating the reoxidation and thus the possible dissolution of Pd within the perovskite framework, typical of the so called “intel-

Table 2  
Fitting of the EXAFS data at the Pd K-edge

Entry	Sample	Shell	CN	<i>R</i> (Å)	$\sigma^2$ (Å <sup>2</sup> )	$\Delta E_0$ (eV)	Residual error (%)
1	PdLCOc8	Pd–O	6.3	2.01	0.003	11.2	8.9
2	PdLCOc8r3	Pd–Pd	6.9	2.73	0.006	1.8	2.8
3	PdLCOc8r3, during reaction at 160 °C	Pd–O	3.5	2.01	0.002	9.8	6.0
4	PdLCOc8r3, after reaction at 500 °C	Pd–Pd	5.0	2.73	0.007	2.5	6.0
5	PdLCOc8r6	Pd–Pd	7.5	2.70	0.007	2.3	3.7
		Pd–Co	4.3	2.70	0.007	6.3	3.7

Note. CN: coordination number; *R*: interatomic distance;  $\sigma^2$ : Debye Waller factor;  $\Delta E_0$ : energy shift.

ligent” catalysts [16]. This is indeed a welcome phenomenon for exhaust gas after-treatment catalysts, because it prevents sintering of Pd particles. (Pd dissolves into the perovskite instead of sintering.) Following a cyclic segregation as small surface clusters during further reduction and redissolution during reoxidation, this behavior confers a longer life to the catalyst compared with the traditional formulation based on Pd supported on silica or alumina. It is worth keeping in mind that in the accompanying paper [32], we showed that after reduction at 300 °C of PdLCOc8, the support reduced to La<sub>2</sub>Co<sub>2</sub>O<sub>5</sub>, but fully reoxidized to LaCoO<sub>3</sub> already at 150 °C in an oxygen-containing atmosphere. Thus PdLCOc8r3 at  $T_{\max} = 160$  °C in the O<sub>2</sub>-rich reaction mixture actually consists of Pd supported on LaCoO<sub>3</sub>. Therefore, despite exhibiting a slightly lower low-temperature activity than PdLCOc8r6, the catalyst prereduced at 300 °C (PdLCOc8r3) must be preferred for practical applications; indeed, it exhibited the aforementioned self-regeneration behavior, permitting simple regeneration by reduction and thus greater durability, as confirmed by our thermal stability test (Fig. 4).

## 5. Conclusion

In the low-temperature selective reduction of NO by H<sub>2</sub> in the presence of excess O<sub>2</sub>, the FP-made Pd/LaCoO<sub>3</sub> catalyst exhibited greater activity and durability than a corresponding sample prepared by the traditional impregnation method. The temperature of precalcination and prereduction strongly affected the catalytic activity of the FP-made Pd/LaCoO<sub>3</sub>. In particular, the best performance was obtained with samples precalcined at 800 °C, followed by reduction. We suggest a cooperative mechanism involving surface Co and Pd particles, leading to the formation of nitrate species on Co, subsequently reduced by hydrogen spillover from Pd. Although reduction at 600 °C gave better catalytic activity, reduction at 300 °C seems preferable, conferring a self-regeneration behavior to the catalyst.

## References

- [1] G. Busca, L. Lietti, G. Ramis, F. Berti, Appl. Catal. B Environ. 18 (1998) 1.
- [2] K. Yokota, M. Fukui, T. Tanaka, Appl. Surf. Sci. 121 (1997) 273.
- [3] B. Frank, G. Emig, A. Renken, Appl. Catal. B Environ. 19 (1998) 45.
- [4] A. Ueda, T. Nakao, M. Azuma, T. Kobayashi, Catal. Today 45 (1998) 135.
- [5] R. Burch, M.D. Coleman, Appl. Catal. B Environ. 23 (1999) 115.
- [6] M. Machida, D. Kurogi, T. Kijima, J. Phys. Chem. B 107 (2003) 196.
- [7] M. Machida, S. Ikeda, J. Catal. 227 (2004) 53.
- [8] T. Nanba, C. Kohno, S. Masukawa, J. Uchisawa, N. Nakayama, A. Obuchi, Appl. Catal. B Environ. 46 (2003) 353.
- [9] G.S. Qi, R.T. Yang, F.C. Rinaldi, J. Catal. 237 (2006) 381.
- [10] C.N. Costa, A.M. Efstathiou, Environ. Chem. Lett. 2 (2004) 55.
- [11] A. Lindstedt, D. Stromberg, M.A. Milh, Appl. Catal. A Gen. 116 (1994) 109.
- [12] D. Ferri, L. Forni, M.A.P. Dekkers, B.E. Nieuwenhuys, Appl. Catal. B Environ. 16 (1998) 339.
- [13] C.N. Costa, V.N. Stathopoulos, V.C. Belessi, A.M. Efstathiou, J. Catal. 197 (2001) 350.
- [14] C.N. Costa, P.G. Savva, C. Andronikou, P.S. Lambrou, K. Polychronopoulou, V.C. Belessi, V.N. Stathopoulos, P.J. Pomonis, A.M. Efstathiou, J. Catal. 209 (2002) 456.
- [15] M. Engelmann-Pirez, P. Granger, G. Leclercq, Catal. Today 107–108 (2005) 315.
- [16] Y. Nishihata, J. Mizuki, T. Akao, H. Tanaka, M. Uenishi, M. Kimura, T. Okamoto, N. Hamada, Nature 418 (2002) 164.
- [17] Y. Nishihata, J. Mizuki, H. Tanaka, M. Uenishi, M. Kimura, J. Phys. Chem. Sol. 66 (2005) 274.
- [18] M. Uenishi, M. Taniguchi, H. Tanaka, M. Kimura, Y. Nishihata, J. Mizuki, T. Kobayashi, Appl. Catal. B Environ. 57 (2005) 267.
- [19] R. Burch, A.A. Shestov, J.A. Sullivan, J. Catal. 188 (1999) 69.
- [20] C.N. Costa, A.M. Efstathiou, J. Phys. Chem. B 108 (2004) 2620.
- [21] A. Snis, I. Panas, Surf. Sci. 413 (1998) 477.
- [22] F. Acke, M. Skoglundh, J. Phys. Chem. B 103 (1999) 972.
- [23] F. Acke, I. Panas, J. Phys. Chem. B 103 (1999) 2195.
- [24] G.L. Chiarello, I. Rossetti, L. Forni, J. Catal. 236 (2005) 251.
- [25] G.L. Chiarello, I. Rossetti, P. Lopinto, G. Migliavacca, L. Forni, Catal. Today 117 (2006) 549.
- [26] R. Strobel, F. Krumeich, W.J. Stark, S.E. Pratsinis, A. Baiker, J. Catal. 222 (2004) 307.
- [27] R. Strobel, L. Madler, M. Piacentini, M. Maciejewski, A. Baiker, S.E. Pratsinis, Chem. Mater. 18 (2006) 2532.
- [28] S. Hannemann, J.D. Grunwaldt, F. Krumeich, P. Kappen, A. Baiker, Appl. Surf. Sci. 252 (2006) 7862.
- [29] L. Fabbrini, A. Kryukov, S. Cappelli, G.L. Chiarello, I. Rossetti, C. Oliva, L. Forni, J. Catal. 232 (2005) 247.
- [30] M. Uenishi, H. Tanaka, M. Taniguchi, I. Tan, Y. Sakamoto, S. Matsunaga, K. Yokota, T. Kobayashi, Appl. Catal. A Gen. 296 (2005) 114.
- [31] C. Oliva, S. Cappelli, A. Kryukov, G.L. Chiarello, A.V. Vishniakov, L. Forni, J. Mol. Catal. A 255 (2006) 36.
- [32] G.L. Chiarello, J.D. Grunwaldt, D. Ferri, F. Krumeich, C. Oliva, L. Forni, A. Baiker, J. Catal. 252 (2007) 127.
- [33] J.D. Grunwaldt, M. Caravati, S. Hannemann, A. Baiker, Phys. Chem. Chem. Phys. 6 (2004) 3037.
- [34] T.J. Ressler, Synchr. Rad. 5 (1998) 118.
- [35] S.I. Zabinsky, J.J. Rehr, A. Ankudinov, R.C. Albers, M.J. Eller, Phys. Rev. B 52 (1995) 2995.
- [36] C.A. de Wolf, B.E. Nieuwenhuys, Surf. Sci. 469 (2000) 196.
- [37] D. Pietrogiaconi, M.C. Campa, S. Tuti, V. Indovina, Appl. Catal. B Environ. 41 (2003) 301.
- [38] L.G. Tejuca, J.L.G. Fierro, Properties and Applications of Perovskite-Type Oxides, Marcel Dekker, New York, 1993.
- [39] J.M.D. Tascón, L.G. Tejuca, C.H. Rochester, J. Catal. 95 (1985) 558.
- [40] M. Kantcheva, A.S. Vakkasoglu, J. Catal. 223 (2004) 352.